Nonlinear Ultrasonic Inspection of Smart CFRP Composites with Embedded PZT Transducers for Space Applications

[1]Christos Andreades, [1]Gian Piero Malfense Fierro, [1]Michele Meo, [2]Francesco Ciampa

[1]Department of Mechanical Engineering, University of Bath, Bath BA2 7AY, UK

[2]Department of Mechanical Engineering Sciences, University of Surrey, Guildford GU2 7XH, UK

Abstract

Carbon fibre reinforced plastic (CFRP) composites used in spacecraft structures are susceptible to delamination, debonds and fibre-cracking that may arise during manufacturing, assembly or in-service operations (e.g. caused by debris impacts in near-Earth orbital spaceflights). Therefore, in-situ and real-time health monitoring is necessary to avoid time-consuming and unsafe visual inspections performed either on-ground or during extra vehicular activities. In this paper, a recently created "smart" CFRP composite structure with embedded piezoelectric (PZT) transducers was used to detect multiple areas of artificial delamination and real impact damage of different size using nonlinear ultrasound. The electrical insulation of embedded PZTs was achieved by interlacing a dry layer of woven glass fibre fabric between the sensor and the CFRP plies before curing. Damage detection was successfully demonstrated using both second harmonic generation and nonlinear modulation (sidebands) of the measured ultrasonic spectrum. The material nonlinear response at the second harmonic and sidebands frequencies was also measured with a laser Doppler vibrometer to validate the nonlinear ultrasonic tests and provide damage localisation. Experimental results revealed that the proposed configuration of embedded PZTs can be utilised for on-board ultrasonic inspection of spacecraft composite parts.

Keywords: Space debris, damage detection, nonlinear ultrasound, composite materials.

1 Introduction

Modern spacecraft structures are made of carbon fibre reinforced plastic (CFRP) composites because of their advantages over metals including high strength-to-weight ratio, fatigue performance, design flexibility and corrosion resistance (Francesconi et al., 1994). CFRP material, for example, offers increased ballistic protection over aluminium when used as the inner wall in dual-wall spacecraft shields (Schonberg, 2017; Schonberg and Walker, 1994). Nevertheless, one of the major problems of CFRP is the susceptibility to damage such as micro-cracks and delamination, which may arise during manufacturing, assembly or in-service operations. In-service defects, in particular, are caused by hypervelocity impacts from micrometeoroids and orbital debris (MMOD) in the near-Earth environment (Schonberg, 2010; Yashiro et al., 2013). Because of the high orbital speed of debris objects (~10 km/s), even sub-millimetres particles can cause severe damage to the spacecraft (Christiansen et al., 2009). Hence, there is a need to provide real-time and in-situ monitoring of material defects at any stage of satellite's component life cycle, especially for the International Space Station and future manned space missions.

Visual inspection is currently the most common technique for inspecting spacecraft components. It relies on the skills and experience of specialised technicians on-ground or astronauts during in-service extravehicular activities (Christiansen, 2003). In the last few decades, material defect identification has also been achieved using a number of different non-destructive evaluation (NDE) methods such as those related to linear ultrasonic wave propagation (Amerini and Meo, 2011; Bricks, 1991), acoustic emission (Cesari et al., 2007; R'Mili et al., 2008; Oskouei and Ahmadi, 2010), thermography (Almond et al., 2017; Holland and Reusser, 2016) and X-ray scanning (Moura and Marques, 2002; Wright et al., 2008). Among NDE methods, ultrasonic technology has the advantage to be simply converted into structural health monitoring (SHM) systems by integrating acoustic/ultrasonic piezoelectric transducers on the monitored component (Aymerich and Staszewski, 2010). Therefore, ultrasonic SHM technology can be used for in-service monitoring of spacecraft structures and it is the focus of this research work. Nonlinear ultrasound, commonly known in the ultrasonic scientific community as nonlinear elastic wave spectroscopy (NEWS) techniques, is a family of ultrasonic inspection methods that have shown higher sensitivity to the detection and localisation of damage (material flaws and micro-cracks) at early stages of formation than linear ultrasound (Boccardi et al., 2018; Su et al., 2006; Zargai et al., 2008). NEWS methods can rely on higher harmonic generation (Buck et al., 1978; Ciampa et al., 2017; Fierro and Meo, 2018; Polimeno et al., 2010; Scarselli et al., 2017; Solodov, 2014), time reversal (Ciampa and Meo, 2012; Lints et al., 2017; Liu et al., 2015), wave modulation (Chrysochoidis et al., 2011; Dionysopoulos et al., 2018; Fierro and Meo, 2018; Klepka et al., 2014; Pieczonka et al., 2015; Van Den Abeele et al., 2000),

phase modulation (Vila et al., 2004), local defect resonance (Post et al., 2017; Segers et al., 2018; Solodov et al., 2015), imaging of nonlinear scatters (Hauper et al., 2017; Solodov and Busse, 2012) and shift in resonance frequency characteristics (Chakrapani et al., 2015; Polimeno and Meo, 2009; Solodov, 2018; Van Den Abeele et al., 2000).

Previous researchers (Aymerich and Staszewski, 2010; Klepka et al., 2015; Liu et al., 2018; Tang et al., 2011), reported damage detection in composite materials by applying NEWS techniques using externally-mounted piezoelectric lead zirconate titanate (PZT) transducers. For spacecraft applications though, there is a strong demand for composite structures with integrated PZTs in order to (i) provide information about micro-cracks during on-ground and in-service ultrasonic monitoring, and (ii) protect the sensors from being directly exposed to the harsh space environment. According to the literature (Mall, 2002; Masmoudi et al., 2015; Paget et al., 2002; Su et al., 2006), both CFRP and glass fibre reinforced plastic (GFRP) composites can include PZTs between the material layers, thus creating "smart" composite structures. However, the integration of PZTs in CFRP composites requires electrical insulation of the transducers from the conductive carbon fibres to avoid short circuits. In previous studies (Mall, 2002; Paget et al., 2002; Su et al., 2006), insulation was achieved by covering the embedded PZTs with layers of polyimide (Kapton) films. However, the embodiment of polymeric films such as Kapton and Teflon between the composite plies is a typical method for constraining ply adhesion and causing artificial delamination (Wooh and Wei, 1999). Consequently, the structural integrity of the composite can be significantly affected by the use of polymeric films.

An innovative material processing technique for the electrical insulation of embedded PZTs in CFRP plates was proposed by the authors in a recent study (Andreades et al., 2018). In particular, a dry layer of woven E-glass fibre fabric was inserted between the conductive surface of the PZTs and the CFRP plies before curing process. This "smart" CFRP composite was subject to mechanical tests including compression, long-beam and short-beam three-point bending tests. An analysis of variance (ANOVA) was conducted on the experimental results and proved that the mean values of compressive, flexural and interlaminar shear strength were equal to the means of plain CFRP specimens. In addition, preliminary NEWS experiments were carried out on the "smart" CFRP composite containing "artificial" delamination simulated by double Teflon patches. The experimental results revealed that the sensitivity to damage based on the amplitude (A_2) of second harmonic generation was nearly twice as high as the sensitivity of surface-bonded PZTs.

The aim of this paper is to further examine the capability of the "smart" CFRP composite with embedded PZTs to detect multiple areas of damage with various dimensions and defect nature. For this scope, NEWS experiments were conducted on two damaged CFRP laminates; one plate with two "artificial" delamination defects (i.e. polymeric film patches) and one plate with real impact flaws.

Artificial damage is generally characterised by debonding at a single interface (in-plane delamination) similarly to delamination caused by manufacturing errors (Smith, 2009). Impacts, on the other hand, usually generate debonding, fibre breakage and matrix cracking at multiple interfaces in the form of through-thickness damage within the laminate (Soutis and Curtis, 1996). In the first part of this paper, defect detection was accomplished based on the second harmonic generation method, whereas in the second part damage identification was achieved using the nonlinear wave modulation technique (see Section 2). In both experimental parts, damage detection at the chosen wave propagation frequency was investigated by scanning the plate surface with a laser Doppler vibrometer (LV) and recording the out-of-plane vibrational velocity surrounding the damage location. The layout of the paper is as follows. In Section 2, the second harmonic generation and the nonlinear wave modulation methods are explained. In Section 3, the manufacture and the damage assessment of CFRP plates along with the NEWS and the LV experiments are outlined. In Section 4, the results from the NEWS and the LV tests are presented. In Section 5, the conclusions of this paper are discussed.

2 Theory

2.1 Second Harmonic Generation

As it is explained by Melchor et al. (2019), the propagation of elastic waves at specific frequencies (single-frequency excitation) through composite materials with cracked matrix, debonded fibres or delaminated plies forces the damaged layers to either oscillate ("clapping" motion) or move relative to each other ("rubbing" motion). This leads to the generation of nonlinear wave effects that can be detected in the form of higher harmonics (even and odd multiples) of the input signal frequency (Ciampa et al., 2017). In particular, second harmonic generation has been reported as the most efficient NEWS feature for damage identification (Landau and Lifshitz, 1986; Munoz et al., 2015). This can be explained by considering the second order nonlinear stress-strain relationship (from Hooke's law)

$$\sigma = E\varepsilon + \frac{E\beta}{2}\varepsilon^2 \tag{1}$$

and the one-dimensional (1D) elastodynamic wave equation

$$\rho \frac{\partial^2 u(x,t)}{\partial t^2} = \frac{\partial \sigma}{\partial x}, \tag{2}$$

where E is the Young's modulus, $\varepsilon = \frac{\partial u(x,t)}{\partial x}$ is the strain, β is the second order nonlinear coefficient (parameter), ρ is the material density, $u(x,t)$ is the displacement (Amura et al., 2011). By substituting equation (1) into equation (2), yields

$$\frac{\partial^2 u(x,t)}{\partial t^2} - c^2 \frac{\partial^2 u(x,t)}{\partial x^2} = \beta c^2 \left(\frac{\partial u(x,t)}{\partial x}\right)\left(\frac{\partial^2 u(x,t)}{\partial x^2}\right), \tag{3}$$

where $c = \sqrt{E/\rho}$ is the longitudinal wave speed. Equation (3) can be then solved using a first-order perturbation method, which has the general solution

$$u(x,t) = u^{(1)}(x,t) + u^{(2)}(x,t)\ , \tag{4}$$

with $u^{(1)} \gg u^{(2)}$. Both linear, $u^{(1)}(x,t)$, and nonlinear, $u^{(2)}(x,t)$, terms can be rewritten as

$$u(x,t) = A_1 \sin(kx - 2\pi ft) - \frac{\beta k^2 A_1^2}{8} x \cos[2(kx - 2\pi ft)]\ , \tag{5}$$

where A_1 is the amplitude of the fundamental frequency harmonic, $A_2 = \frac{\beta k^2 A_1^2}{8} x$ is the amplitude of the second harmonic wave associated with the nonlinear material behaviour, x is the wave propagation distance within the material and k is the wave number (Amura et al., 2011).

2.2 Nonlinear Wave Modulation

In the case of multiple-frequency excitation of damaged composite materials, further nonlinear wave effects are generated due to the interaction of the propagating waves with the damage. When a damaged material is excited using two continuous periodic waves, one with a low frequency (f_1) and one with a high frequency (f_2), the damage behaves as a multiplier and mixer of the two excitation frequencies. The amplitude of the high frequency wave is modulated by the low frequency one and, in addition to higher harmonics, intermodulation products (sidebands) can be generated in the frequency spectrum of the received signal at frequencies equal to $f_2 \pm nf_1$, where n is a positive integer (Fierro, 2014). Undamaged (intact) materials are, instead, characterised by a linear response as the elastic waves are not interacting with any damage. Therefore, only the fundamental frequencies (f_1 and f_2) are detectable in the frequency domain of the received signal (Meo et al., 2008). Nonlinear wave modulation method has also been proved to be effective for defect detection (Chrysochoidis et al., 2011; Dionysopoulos et al., 2018; Klepka et al., 2014; Pieczonka et al., 2015). Similarly to the second harmonic generation, equation (3) can be solved with dual periodic excitation using the first-order perturbation method, and the amplitudes A_+ and A_- associated to each sideband $f_+ = f_2 + f_1$ and $f_- = f_2 - f_1$ can be expressed as

$$A_+ = \frac{\beta_+ k_{f_1} k_{f_2} A_{f_1} A_{f_2}}{4} x \tag{6}$$

and

$$A_- = \frac{\beta_- k_{f_1} k_{f_2} A_{f_1} A_{f_2}}{4} x \tag{7}$$

where A_{f_1} and A_{f_2} are the amplitudes and k_{f_1} and k_{f_2} are the wave numbers of the input signals at f_1 and f_2 frequencies, respectively, and β_+ and β_- are the nonlinear parameters (Fierro and Meo, 2015).

3 Experimentation

3.1 Manufacture of CFRP Plates

A total of three carbon/epoxy (T800/M21) laminates with dimensions of 180 x 140 x 3.5 mm were used in the experiments of this study. The laminates were made from unidirectional prepreg layers with a [90°/0°/90°/0°/90°/0°]s lay-up, and they were cured in an autoclave for 180 minutes at a pressure of 0.7 MPa and a temperature of 150°C with a ramp rate of 3°C/min. As illustrated in Figure 1, all three plates included two embedded PZTs (ferroelectric soft piezo material PIC 255) of 6 mm diameter and 0.3mm thickness, for the propagation of ultrasonic elastic waves. A 10 x 10 mm layer of woven E-glass fibre fabric was also interlaced between the top surface of the PZTs and the CFRP plies, for electrical insulation. The PZTs were directly placed between the 8th and the 9th layers from the bottom. The thin wires from to the positive and negative electrodes of the PZTs were connected to 50 Ω straight Bayonet Neill-Concelman (BNC) plugs through low noise cables (RG174/U). The wires were directed outside the top surface of the plate through small slits in the fibre direction of every CFRP ply (i.e. without cutting any fibres).

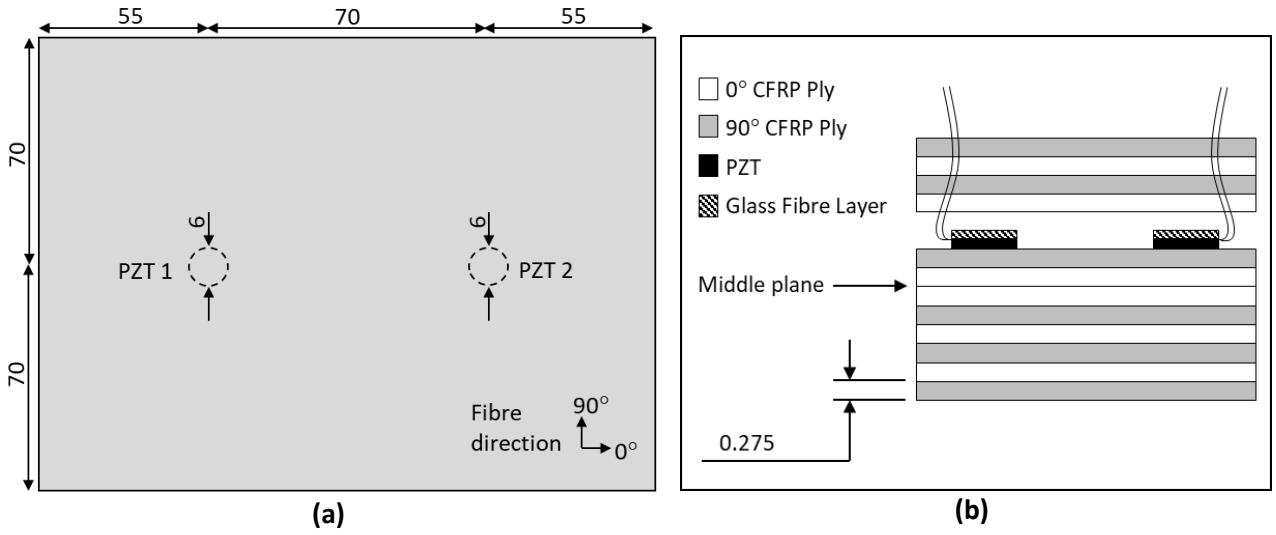

Figure 1: Design of undamaged CFRP plate - top view (a) and stacking sequence (b). Dimensions in mm. Not to scale.

3.2 Damage Assessment and Sensor Functionality

The first laminate (Figure 1) was kept intact and used as the reference plate. The second laminate (Figure 2a) included two double-layered patches of different size to cause controlled artificial in-plane delamination. Each patch consisted of two square layers of 12 μm thick Fluorinated Ethylene Propylene (FEP) film stacked one on top of the other. The FEP patches were inserted at the same plane of the PZTs (between layers 8 and 9 from the bottom). The third plate (Figure 2b) was impacted at its centre with a hemispherical indentor of 20 mm diameter. The damage was initially created with

an impact energy of 10 J and, once the experimental detection was completed, the damage size was increased with another impact of higher energy (15 J). In the following paragraphs, the first plate is referred as the undamaged (UD) laminate, and the second and third plates as the artificially damaged (AD) and the impact damaged (ID) laminates respectively.

It must be noted that the capacitance of the PZTs was measured with the use of a Keithley 2110 5 1/2 multimeter before their embedment in the composite plates, after the curing process of the plates, and after impacting the ID-laminate. In all cases, the capacitance was the same (1.54±0.02 nF) suggesting that the PZTs were functional. This is a typical sensor inspection method in literature (Konka et al., 2012; Yoo et al., 2014). In fact, any noticeable drop in capacitance would indicate cracking or depoling of the transducer from either the high curing pressure and temperature or the applied impact load.

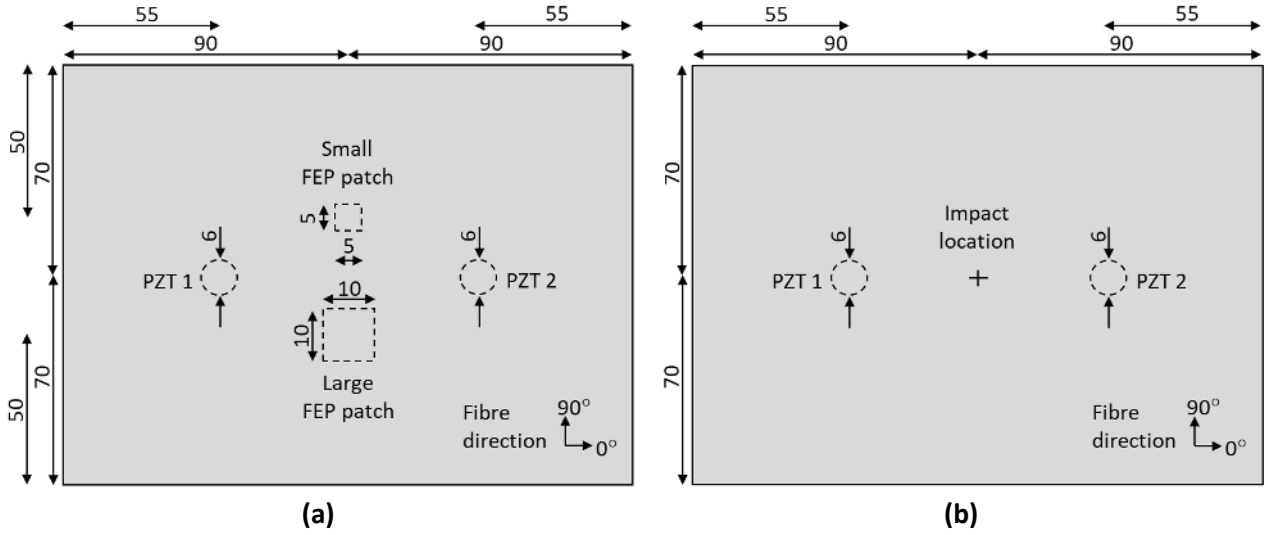

Figure 2: Design of artificially damaged plate (a) and impact damaged plate (b). Dimensions in mm. Not to scale.

Prior to performing any experiment, the size of the damage in AD- and ID- plates was evaluated by conducting stepped linear C-scans using a phased array system (Diagnostic Sonar Ltd) equipped with a 5 MHz probe containing 128 elements. More specifically, the C-scans were carried out in steps of 12 elements (single cycle pulse, element pitch of 0.52 mm) and the damage was assessed based on the signal amplitude. The front face of the probe included a 30 mm acrylic (Perspex) delay line and coupling was achieved using ultrasonic gel. As shown in Figure 3 and Figure 4, the areas at which delamination was detected matched the positions of the double FEP patches and the impact damage. In the AD-plate, the two defects had a similar size to that of the double FEP patches. In the ID-plate, the initial damage diameter (10 J impact) was approximately 18 mm, and the final diameter (15 J impact) was around 32 mm.

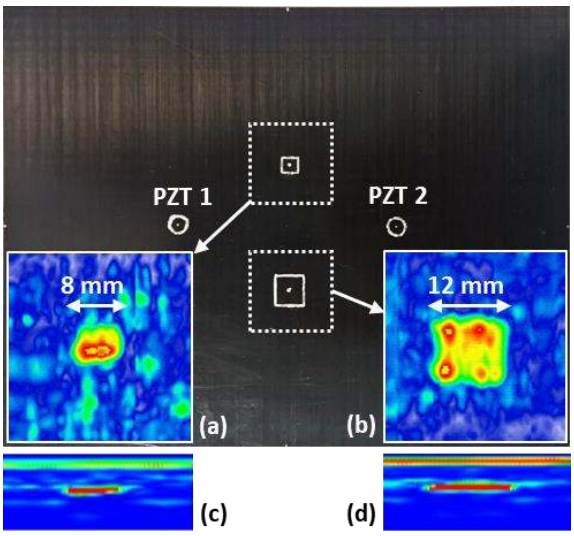

Figure 3: Ultrasonic C-scan of the small (a) and the big (b) artificial damage in AD-laminate and the associated B-scans (c), (d) - Images not to scale.

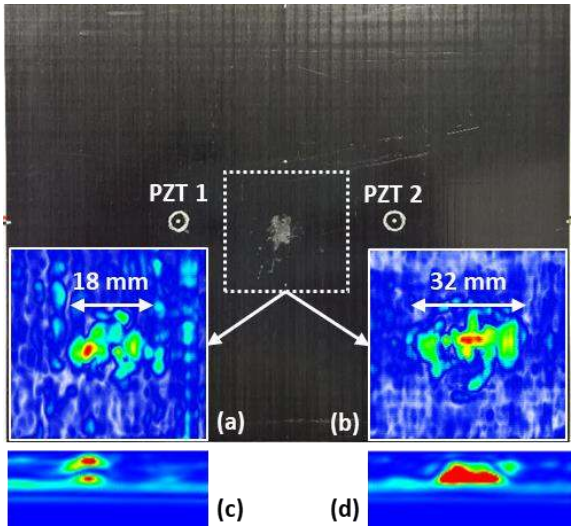

Figure 4: Ultrasonic C-scan of the 10 J (a) and the 15 J (b) impact damage in ID-laminate and the associated B-scans (c), (d) - Images not to scale.

3.3 Experimental Set-up and Method

3.3.1 NEWS Experiments

Starting from the NEWS experiments based on the second harmonic generation method, in each CFRP plate PZT1 was used for the transmission and PZT2 for the reception of continuous periodic ultrasonic signals (i.e. single-frequency excitation). As illustrated in Figure 5 below, the input signal was generated from an arbitrary waveform generator (TTi TGA12104) and its amplitude was increased using a voltage amplifier (Falco Systems WMA-300). The received signal was monitored in the time and frequency domains at a sampling frequency of 2 MHz and a total acquisition time of 50 ms using an oscilloscope (PicoScope 4424). Initially, in the AD- and ID-laminates the input signal frequency of PZT1 was swept between 20 and 500 kHz to determine the two frequencies

corresponding to the highest A_2 amplitudes of the received signal. In the case of the AD-plate, the two chosen frequencies were very likely to be associated with the excitation of the two FEP patches, whereas for the ID-plate, the chosen frequencies were related to the excitation of the damage caused initially with 10 J, and then with 15 J of impact energy. At these four frequencies, the amplitude of the fundamental (A_1) and A_2 harmonics was recorded for input signal voltages of 60, 70, 80, 90 and 100 V. It must be noted that the chosen input signal frequencies would not necessarily correspond to the highest A_1 amplitude as this is highly dependent on the excitation of the PZT1 and the tested material. For clarity, Table 1 summaries the input frequencies and voltages used with the PZT1. The UD-plate was also excited at the same four frequencies and its ultrasonic response was compared to the damaged samples.

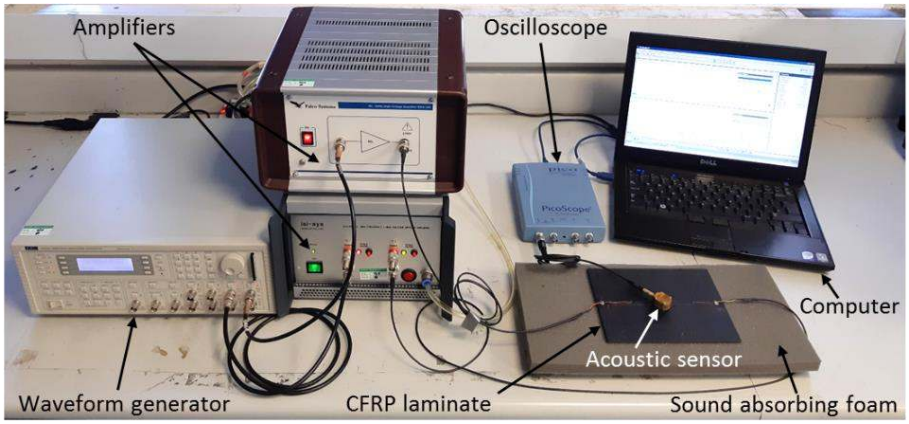

Figure 5: Illustration of the set-up used in NEWS experiments.

Table 1: Input signal frequencies and voltages used in NEWS experiments for second harmonic generation.

CFRP Plate	Sweep analysis freq. band - PZT1 (kHz)	Input volt. to PZT1 (V)	Chosen damage excitation freq. (kHz)
AD	20-500	60, 70, 80, 90, 100	f_1=104.5, 184.7
ID	20-500	60, 70, 80, 90, 100	f_1=128, 310

For the NEWS experiments associated with the nonlinear wave modulation technique, both embedded PZTs were used to excite the ID- and UD-laminates (i.e. multiple-frequency excitation). In each plate, PZT1 was used to send ultrasonic waves at low frequency (f_1) whereas PZT2 enabled high frequency (f_2) transmission. According to Figure 5, PZT1 was connected to a channel of the waveform generator through the Falco Systems WMA-300 amplifier and PZT2 was powered by a separate channel through an ISI-SYS HVA-B100-2 amplifier. The propagating waves were received using an external acoustic transducer (McWade 300 kHz NS3303) connected to the oscilloscope. In

the ID-plate, PZT1 was swept between 10-50 kHz and the f_1 values associated with the five highest peaks of the received signal amplitude were recorded. For every f_1 value, PZT2 was swept between 100-300 kHz and the frequency spectrum of the received signal was examined in order to determine the combination of f_1 and f_2 which results in the strongest wave modulation, based on the amplitude of the sidebands. By keeping the input voltage to PZT2 constant at 50 V and increasing the input voltage to PZT1 from 60 to 100 V in steps of 10 V, the received signal amplitude was recorded at f_1, f_2 and $f_2 \pm f_1$ frequencies. A summary of the input signal frequencies and voltages to the PZT1 and PZT2 in the ID-plate is provided in Table 2, together with the frequencies found to cause damage excitation. The UD-plate was also subject to multiple-frequency excitation using the chosen f_1 and f_2 frequencies.

Table 2: Input signal frequencies and voltages used in NEWS experiments for nonlinear wave modulation.

CFRP Plate	Sweep analysis freq. band - PZT1 (kHz)	Input volt. to PZT1 (V)	Sweep analysis freq. band - PZT2 (kHz)	Input volt. to PZT2 (V)	Chosen damage excitation freq. (kHz)
ID	10-50	60, 70, 80, 90, 100	100-300	50	f_1=18 f_2=192

3.3.2 LV Experiments

In both NEWS experiments with second harmonic and sidebands generation, a series of LV experiments were performed to examine whether the generation of second harmonics and the presence of sidebands at the chosen input signal frequencies was actually attributed to the damage excitation. As shown in Figure 6, ultrasonic waves were transmitted from the same PZTs as described in Section 3.3.1, using the same configuration of arbitrary waveform channels and amplifiers. Second harmonic generation in the AD- and ID-plate was studied by measuring the out-of-plane vibrational velocity of the plate surface at A_1 and A_2 frequencies, using the LV scanning head (Polytec PSV-400). The input signal voltage applied to PZT1 was fixed at 300 V. Similarly, nonlinear wave modulation in the ID-plate was investigated by applying input voltages of 100 V and 300 V to the PZT1 and PZT2 respectively, and recording the vibrational velocity of the plate surface at f_1, f_2 and $f_2 \pm f_1$ frequencies.

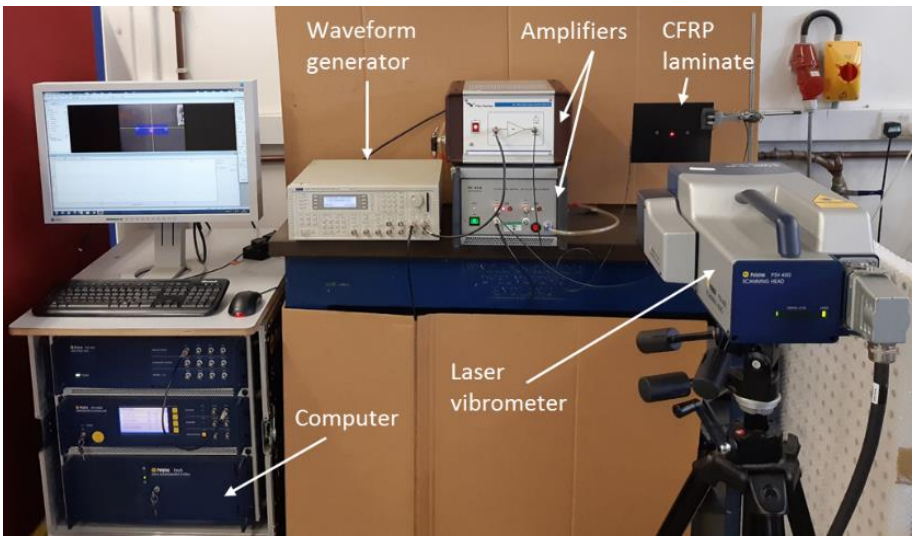

Figure 6: Illustration of the set-up used in LV experiments.

4 Results and Discussion

4.1 Second Harmonic Generation Experiments

As explained in Section 3.3.1, by sweeping the frequency of PZT1 in the AD-plate from 20 to 500 kHz, the two highest A_2 amplitudes were observed at 104.5 kHz and 184.7 kHz frequencies. Hence, these two were considered as the frequencies causing the strongest excitation of the two FEP patches. Similarly, in the ID-plate, the two input signal frequencies related to the excitation of the 10 J and the 15 J impact damage were chosen at 310 kHz and 128 kHz, respectively, based on the A_2 amplitude. After exciting the UD-laminate at these four frequencies, A_2 harmonics were not found in the frequency spectrum, thus verifying that the plate was intact. An example is presented in Figure 7. Additionally, the A_1 amplitude in the case of the UD-plate was always greater than in the damaged laminates. That was expected as in the damaged laminates part of the transmitted wave energy was transferred from the fundamental input wave to the nonlinear harmonic one. Moreover, as can be seen in Figure 8 and Figure 9, the results obtained from the AD- and ID-plates indicated that by increasing the input voltage to PZT1 from 60 to 100 V, the received signal amplitude at A_1 and A_2 frequencies was also rising. The A_2 amplitude was around two orders of magnitude smaller than the A_1 amplitude, in both plates.

Furthermore, three-dimensional plots of the results obtained from the LV experiments on AD- and ID-laminates (Figure 10 and Figure 11) confirmed that the out-of-plane vibrational velocity was always higher at the location of the impact. The A_2 amplitude was about an order of magnitude smaller than the A_1 amplitude. The LV experiments on the AD-laminate showed that the input signal at 104.5 kHz caused excitation only to the big FEP patch and, at 184.7 kHz, only to the small FEP patch. Similarly, the 10 J impact damage in the ID-laminate was only excited at 310 kHz, and after

the second impact of 15 J only at 128 kHz. This verified the correct selection of damage excitation frequencies.

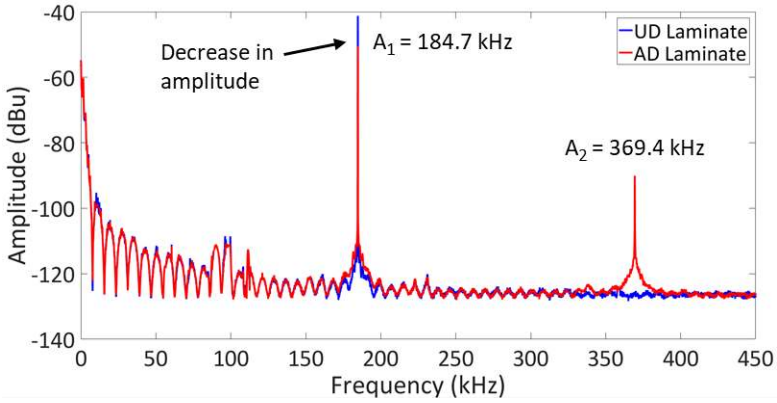

Figure 7: Frequency spectrum of the received signal in the UD-laminate and in the AD-laminate - Input signal of 60 V at 184.7 kHz.

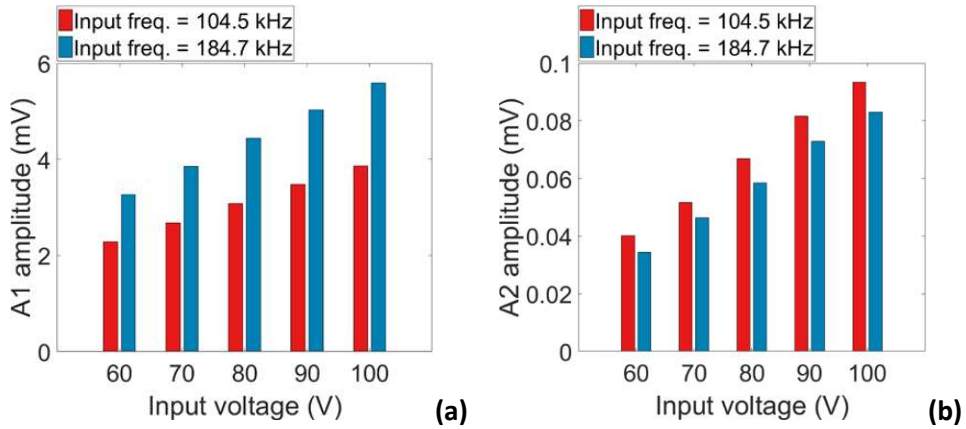

Figure 8: Amplitude of the received signal in AD-laminate at the fundamental (a) and second (b) harmonic frequencies - Input signals of 60, 70, 80, 90, and 100 V at 104.5 and 184.7 kHz.

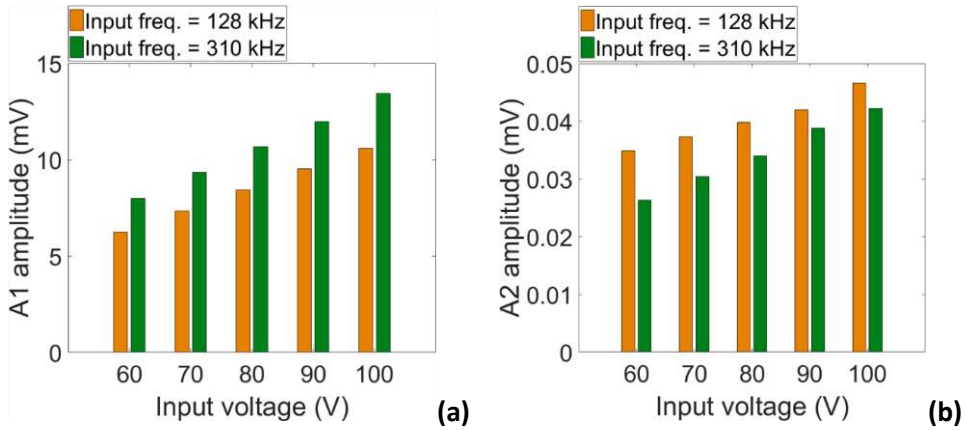

Figure 9: Amplitude of the received signal in ID-laminate at the fundamental (a) and second (b) harmonic frequencies - Input signals of 60, 70, 80, 90, and 100 V at 128 and 310 kHz.

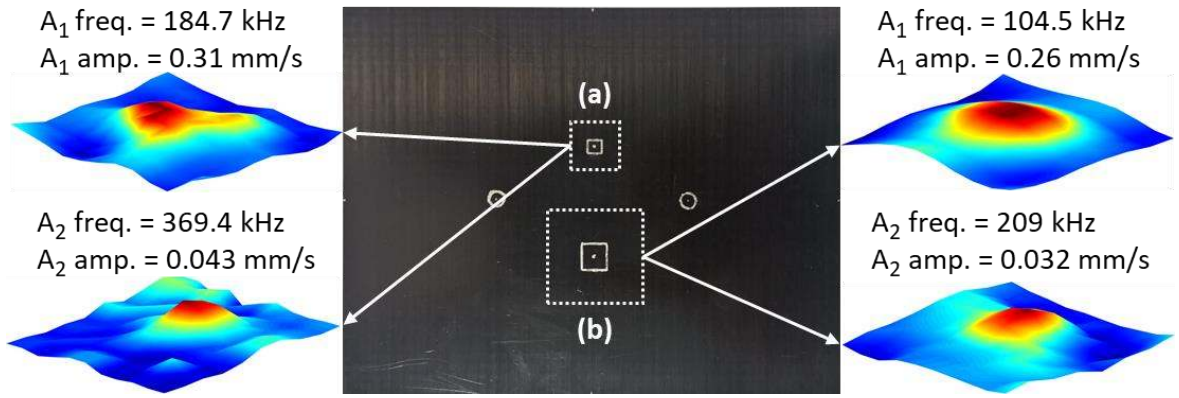

Figure 10: 3D representation of the out-of-plane vibrational velocity around the location of the small (a) and the big (b) artificial damage at the fundamental and second harmonic frequencies.

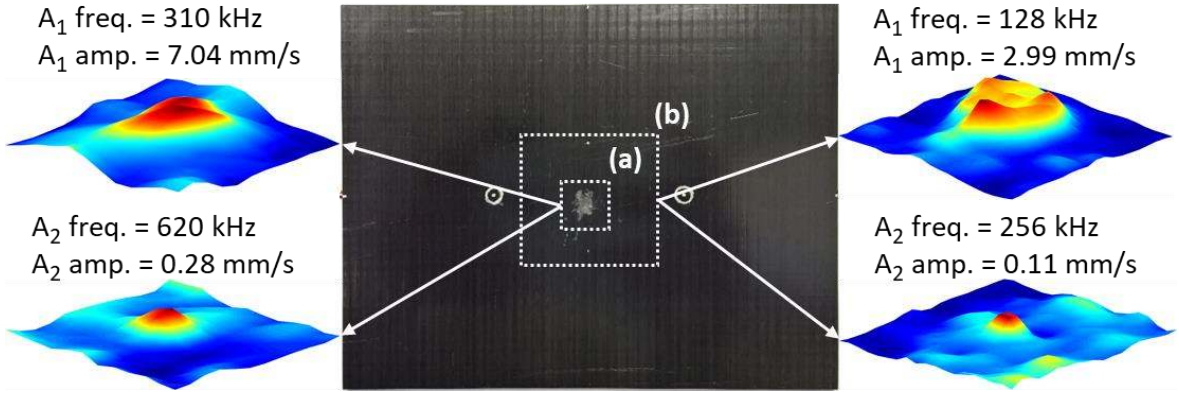

Figure 11: 3D representation of the out-of-plane vibrational velocity around the location of the 10 J (a) and the 15 J (b) impact damage at the fundamental and second harmonic frequencies.

4.2 Nonlinear Wave Modulation Experiment

According to the process described in Section 3.3.1 and based on the amplitude of the sidebands in the ultrasonic response of the ID-plate, the effect of nonlinear wave modulation was evaluated by transmitting periodic waves from PZT1 at f_1=18 kHz and from PZT2 at f_2=192 kHz. The UD-laminate was also subject to multiple-frequency using the same f_1 and f_2 frequencies. For an input voltage of 60 V applied to PZT1 and 50 V applied to PZT2, the received signal amplitude at 18 kHz and 192 kHz was lower in the case of the ID-plate (Figure 12). As previously explained, that was reasonable because an amount of the input wave energy was transferred from the f_1 and f_2 signals to the sidebands. In addition, first-order sidebands were only presented in the spectrum of the ID-laminate at 174 kHz ($f_- = f_2 - f_1$) and 210 kHz ($f_+ = f_2 + f_1$), and this confirm its nonlinear response under wave modulation. Also, in the ID-plate, by increasing the input voltage to PZT1 from 60 to 100 V and keeping the input voltage to PZT2 constant at 50 V, the amplitude of the f_1 harmonic and the two sidebands increased proportionally by around 70%, whereas the amplitude of f_2 harmonic

remained almost constant (Figure 13). This verified that the existence of sidebands was attributed to the wave modulation by the f_1 signal. For all five values of the input voltage, the amplitude of sidebands was three orders of magnitude smaller than the amplitude of f_2 harmonic and one order of magnitude smaller than the amplitude of f_1 harmonic. The amplitude of the right sideband f_+ was on average 27% greater than the left one f_-.

Regarding to the LV experiments, the three-dimensional plots of the results illustrated in Figure 14 proved that the out-of-plane vibrational velocity at f_1, f_2, f_+ and f_- was always higher at the impact location. These results were in agreement with the results from the NEWS experiments with respect to the amplitude difference between the sidebands and the f_1, f_2 harmonics. Particularly, the amplitude of the right sideband, f_+, was around 30% greater than the amplitude of the left one, f_-. Moreover, the amplitude of both sidebands was two orders of magnitude smaller than the amplitude of the f_2 harmonic and one order of magnitude smaller than the amplitude of the f_1 harmonic. Hence, the LV experiments confirmed that the detection of intermodulation products was associated with the nonlinear elastic behaviour of the damaged plate.

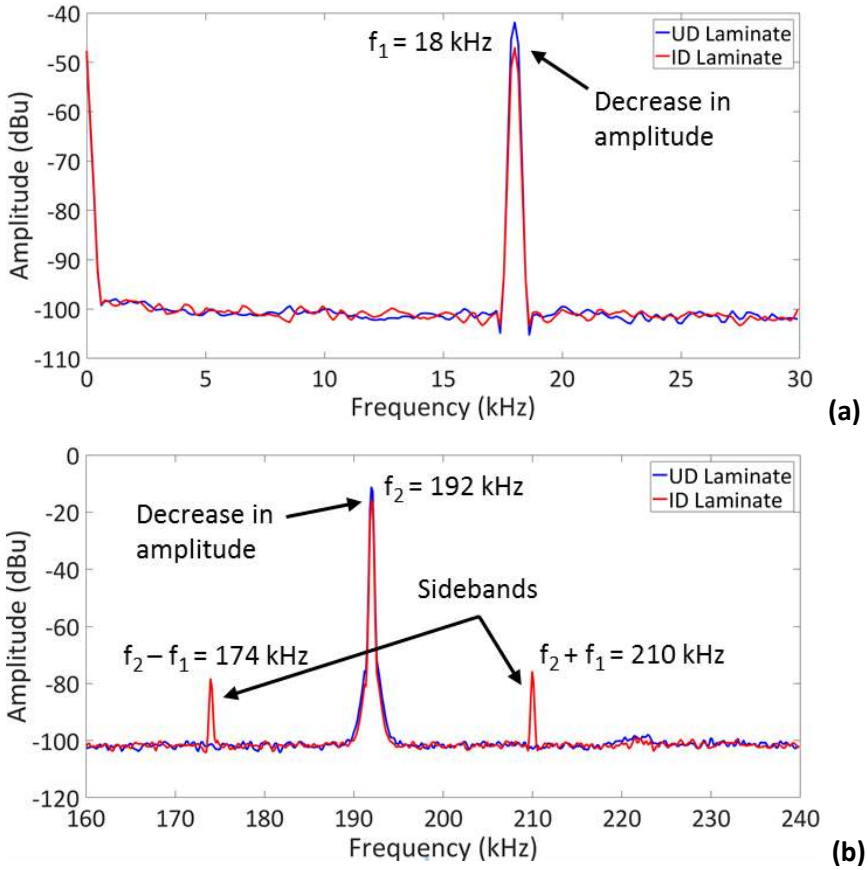

Figure 12: Amplitude of the received signal in the UD-laminate and the ID-laminate at $\boldsymbol{f_1}$ (a) and at $\boldsymbol{f_2}$ and $\boldsymbol{f_2 \pm f_1}$ (b) - Input signal voltage to PZT2 = 50 V and to PZT1 = 60 V.

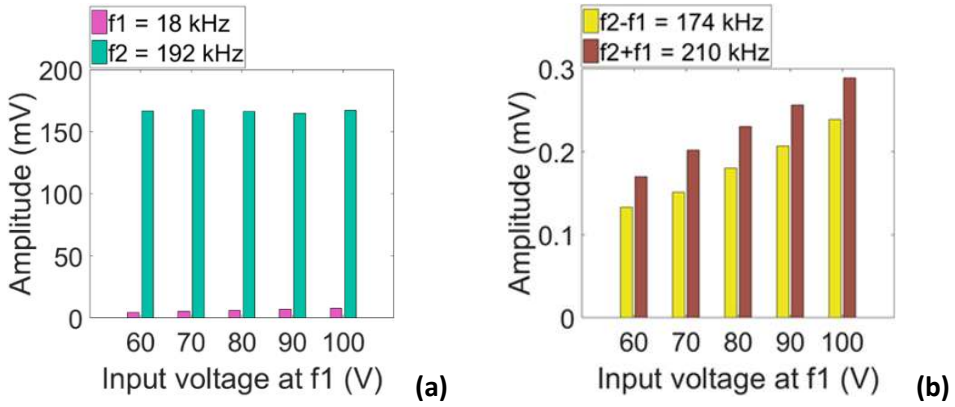

Figure 13: Amplitude of the received signal in the ID-laminate at f_1 & f_2 (a) and at $f_2 \pm f_1$ (b) - Input signal voltage to PZT2 = 50 V and to PZT1 = 60, 70, 80, 90 and 100 V.

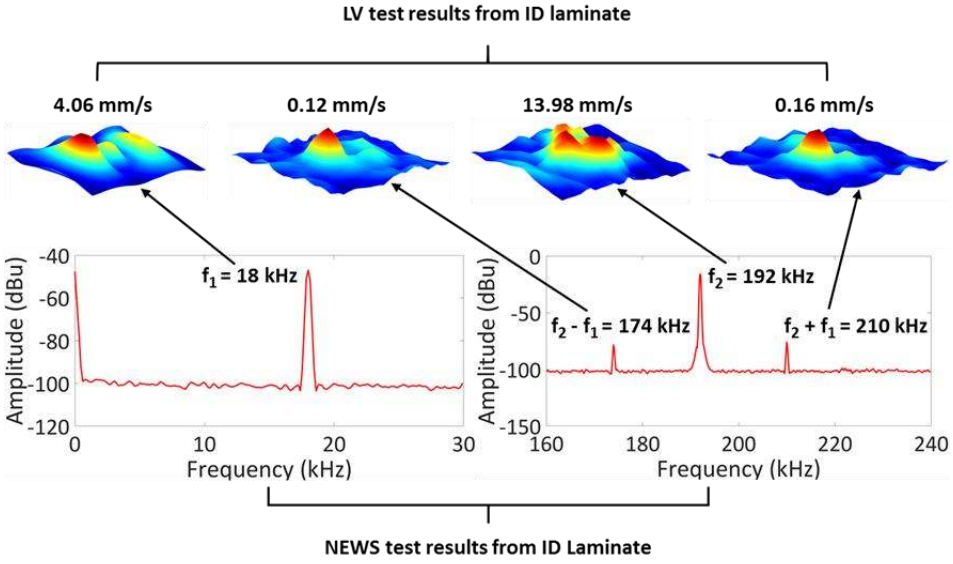

Figure 14: 3D representation of the out-of-plane vibrational velocity at the location of the impact damage at f_1, f_2 and $f_2 \pm f_1$.

5 Conclusions

The aim of this study was to demonstrate the damage detection capabilities of directly embedded PZTs in CFRP composites with nonlinear ultrasound. PZTs were electrically insulated using a novel embedding technique in which the conductive surface of each transducer was covered by a single layer of woven E-glass fibre fabric. The ultrasonic response of CFRP plates with areas of artificial (polymeric film patches) and real (impact) damage of different size was compared with the response of an intact plate, using pairs of embedded PZTs. In the first part of experiments, one PZT was used as the transmitter and the other as the receiver of ultrasonic elastic waves. Excitation of each damage type (artificial and impact) was achieved at a different input signal frequency. This was detected based on the generation of A_2 harmonics in the frequency spectrum of the received signal, and the amplitude of these harmonics was found to increase with increasing input signal voltage. Furthermore, by using

an LV, the out-of-plane vibration velocity of the laminate surface was also recorded at A_1 and A_2 frequencies and found to be greater at the damage location. In the second experimental part, nonlinear wave modulation was employed for defect detection. The undamaged and impacted plates were excited by ultrasonic waves transmitted from both PZTs at different frequencies (f_1 and f_2). An external transducer was used as the receiver. The nonlinear response of the impacted laminate was verified by the presence of first-order sidebands ($f_+ = f_2 + f_1$ and $f_- = f_2 - f_1$) in the frequency spectrum of the received signal, and the amplitude of sidebands was increasing with rising input voltage at f_1. Again, by scanning the material response at f_1, f_2, f_+ and f_- frequencies with the LV, the out-of-plane vibrational velocity of the laminate surface was confirmed higher at the impact location. The experimental results revealed that multiple damage locations of different size in composite laminates were successfully detected. Moreover, it was demonstrated that these embedded PZTs were capable of detecting in-plane delamination which is usually related to manufacturing errors, but also through-thickness damage (multi-layer fibre and matrix cracking) that commonly occur after impacts. Therefore, it is concluded that the proposed configuration of embedded PZTs has the potential to be used for the development of "smart" composite structures to enable in-situ and real-time ultrasonic inspection of satellite components. Future challenges are to implement optimal signal transmission/reception and data storage strategies for real satellite operations in order to make the proposed NEWS technology with embedded PZT transducers compliant with other spacecraft sub-systems.

Acknowledgements

Francesco Ciampa acknowledges the Royal Society-Newton Mobility Grant (IEC\NSFC\170387) project and Michele Meo acknowledges the Horizon 2020 "EXTREME" project to support this research work.

References

1. Almond DP, Angioni SL and Pickering SG (2017) Long pulse excitation thermographic non-destructive evaluation. *NDT & E International* 87(1): 7-14.
2. Amerini F and Meo M (2011) Structural health monitoring of bolted joints using linear and nonlinear acoustic/ultrasound methods. *Structural Health Monitoring* 10(6): 659-672.
3. Amura M, Meo M and Amerini F (2011) Baseline-free estimation of residual fatigue life using a third order acoustic nonlinear parameter. *The Journal of the Acoustical Society of America* 130(4): 1829-1837.

4. Andreades C, Mahmoodi P and Ciampa F (2018) Characterisation of smart CFRP composites with embedded PZT transducers for nonlinear ultrasonic applications. *Composite Structures* 206(1): 456-466.
5. Aymerich F and Staszewski WJ (2010) Impact damage detection in composite laminates using nonlinear acoustics. *Composites Part A: Applied Science and Manufacturing* 41(9): 1084-1092.
6. Boccardi S, Calla DB, Ciampa F, et al. (2018) Nonlinear elastic multi-path reciprocal method for damage localisation in composite materials. *Ultrasonics* 82(1): 239-245.
7. Briks AS and Green R E (1991) *Nondestructive Testing Handbook: Ultrasonic Testing*. Ohio: American Society for Nondestructive Testing.
8. Buck O, Morris WL and Richardson JM (1978) Acoustic harmonic generation at unbonded interfaces and fatigue cracks. *Applied Physics Letters* 33(5): 371-372.
9. Cesari F, Dal Re V, Minak G, et al. (2007) Damage and residual strength of laminated carbon-epoxy composite circular plates loaded at the centre. *Composites Part A: Applied Science and Manufacturing* 38(4): 1163-1173.
10. Chakrapani SK, Barnard DJ and Dayal V (2015) Influence of fiber orientation on the inherent acoustic nonlinearity in carbon fiber reinforced composites. *The Journal of the Acoustical Society of America* 137(2): 617-624.
11. Christiansen EL (2003) *Meteoroid/debris shielding*. Houston: National Aeronautics and Space Administration, Lyndon B. Johnson Space Center, pp. 75-76.
12. Christiansen EL, Arnold J and Corsaro B (2009) Handbook for designing MMOD protection. *NASA Johnson Space Center*. NASA/TM-2009-214785.
13. Chrysochoidis NA, Barouni AK and Saravanos DA (2011) Delamination detection in composites using wave modulation spectroscopy with a novel active nonlinear acousto-ultrasonic piezoelectric sensor. *Journal of Intelligent Material Systems and Structures* 22(18): 2193-2206.
14. Ciampa F and Meo M (2012) Nonlinear elastic imaging using reciprocal time reversal and third order symmetry analysis. *The Journal of the Acoustical Society of America* 131(6): 4316-4323.
15. Ciampa F, Pickering SG, Scarselli G, et al. (2017) Nonlinear imaging of damage in composite structures using sparse ultrasonic sensor arrays. *Structural Control and Health Monitoring* 24(5): 1911.
16. Ciampa F, Scarselli G and Meo M (2017) On the generation of nonlinear damage resonance intermodulation for elastic wave spectroscopy. *The Journal of the Acoustical Society of America* 141(4): 2364-2374.

17. Dionysopoulos D, Fierro GPM, Meo M, et al. (2018) Imaging of barely visible impact damage on a composite panel using nonlinear wave modulation thermography. *NDT & E International* 95(1): 9-16.
18. Fierro GPM (2014) *Development of Nonlinear Ultrasound Techniques for Multidisciplinary Engineering Applications*. PhD Thesis, University of Bath, UK.
19. Fierro GPM and Meo M (2015) Residual fatigue life estimation using a nonlinear ultrasound modulation method. *Smart Materials and Structures* 24(2): 025040.
20. Fierro GPM and Meo M (2018) Structural health monitoring of the loosening in a multi-bolt structure using linear and modulated nonlinear ultrasound acoustic moments approach. *Structural Health Monitoring* 17(6): 1475921718806141.
21. Fierro GPM and Meo M (2019) A combined linear and nonlinear ultrasound time-domain approach for impact damage detection in composite structures using a constructive nonlinear array technique. *Ultrasonics* 93(1): 43-62.
22. Francesconi A, Giacomuzzo C, Kibe S et al. (2012) Effects of high-speed impacts on CFRP plates for space applications. *Advances in Space Research* 50(5): 539-548.
23. Haupert S, Renaud G and Schumm A (2017) Ultrasonic imaging of nonlinear scatterers buried in a medium. *NDT & E International* 87(1): 1-6.
24. Holland SD and Reusser RS (2016) Material evaluation by infrared thermography. *Annual Review of Materials Research* 46(1): 287-303.
25. Klepka A, Pieczonka L, Staszewski WJ, et al. (2014) Impact damage detection in laminated composites by non-linear vibro-acoustic wave modulations. *Composites Part B: Engineering* 65(1): 99-108.
26. Klepka A, Staczkiewicz M, Pieczonka L, et al. (2015) Triple correlation for detection of damage-related nonlinearities in composite structures. *Nonlinear Dynamics* 81(1-2): 453-468.
27. Konka HP, Wahab MA and Lian K (2012) On mechanical properties of composite sandwich structures with embedded piezoelectric fiber composite sensors. *Journal of Engineering Materials and Technology* 134(1): 011010.
28. Landau LD and Lifshitz EM (1986) *Theory of Elasticity*. Oxford: Butterworth-Heinemann.
29. Lints M, Dos Santos S and Salupere A (2017) Solitary waves for non-destructive testing applications: Delayed nonlinear time reversal signal processing optimization. *Wave Motion* 71(1): 101-112.
30. Liu X, Bo L, Yang K, et al. (2018) Locating and imaging contact delamination based on chaotic detection of nonlinear Lamb waves. *Mechanical Systems and Signal Processing* 109(1) 58-73.

31. Liu Z, Yu H, Fan J, et al. (2015) Baseline-free delamination inspection in composite plates by synthesizing non-contact air-coupled Lamb wave scan method and virtual time reversal algorithm. *Smart Materials and Structures* 24(4): 045014.
32. Mall S (2002) Integrity of graphite/epoxy laminate embedded with piezoelectric sensor/actuator under monotonic and fatigue loads. *Smart Materials and Structures* 11(4): 527-533.
33. Masmoudi S, El Mahi A and Turki S (2015) Use of piezoelectric as acoustic emission sensor for in situ monitoring of composite structures. *Composites Part B: Engineering* 80(1): 307-320.
34. Melchor J, Parnell WJ, Bochud N, et al. (2019) Damage prediction via nonlinear ultrasound: A micro-mechanical approach. *Ultrasonics* 93(1): 145-155.
35. Meo M, Polimeno U and Zumpano G (2008) Detecting damage in composite material using nonlinear elastic wave spectroscopy methods. *Applied Composite Materials* 15(3): 115-126.
36. Moura MF and Marques AT (2002) Prediction of low velocity impact damage in carbon-epoxy laminates. *Composites Part A: Applied Science and Manufacturing* 33(3): 361-368.
37. Munoz R, Bochud N, Rus G et al. (2015) Model-based damage evaluation of layered CFRP structures. In: *41st Annual Review of Progress in Quantitative Nondestructive Evaluation* (ed DE Chimenti and LJ Bond), Boise, Idaho, 20-25 July 2014, pp.1170-1177. New York: AIP Publishing.
38. Oskouei AR and Ahmadi M (2010) Acoustic emission characteristics of mode I delamination in glass/polyester composites. *Journal of composite materials* 44(7): 793-807.
39. Paget CA, Levin K and Delebarre C (2002) Actuation performance of embedded piezoceramic transducer in mechanically loaded composites. *Smart Materials and Structures* 11(6): 886-891.
40. Pieczonka L, Klepka A, Martowicz A, et al. (2015) Nonlinear vibroacoustic wave modulations for structural damage detection: an overview. *Optical Engineering* 55(1): 011005.
41. Polimeno U and Meo M (2009) Detecting barely visible impact damage detection on aircraft composites structures. *Composite structures* 91(4): 398-402.
42. Polimeno U, Meo M, Almond DP, et al. (2010) Detecting low velocity impact damage in composite plate using nonlinear acoustic/ultrasound methods. *Applied Composite Materials* 17(5):481-488.
43. Post W, Kersemans M, Solodov I, et al. (2017) Non-destructive monitoring of delamination healing of a CFRP composite with a thermoplastic ionomer interlayer. *Composites Part A: Applied Science and Manufacturing* 101(1): 243-253.
44. R'Mili M, Moevus M and Godin N (2008) Statistical fracture of E-glass fibres using a bundle tensile test and acoustic emission monitoring. *Composites Science and Technology* 68(7): 1800-1808.

45. Scarselli G, Ciampa F, Nicassio F, et al. (2017) Non-linear methods based on ultrasonic waves to analyse disbonds in single lap joints. *Proceedings of the Institution of Mechanical Engineers, Part C: Journal of Mechanical Engineering Science* 231(16): 3066-3076.
46. Schonberg WP (2010) Protecting Earth-orbiting spacecraft against micro-meteoroid/orbital debris impact damage using composite structural systems and materials: An overview. *Advances in Space Research* 45(6): 709-720.
47. Schonberg WP (2017) Studies of hypervelocity impact phenomena as applied to the protection of spacecraft operating in the MMOD environment. *Procedia Engineering* 204(1): 4-42.
48. Schonberg WP and Walker EJ (1994) Hypervelocity impact of dual-wall space structures with graphite/epoxy inner wall. *Composites Engineering* 4(10): 1045-1054.
49. Segers J, Kersemans M, Hedayatrasa S, et al. (2018) Towards in-plane local defect resonance for non-destructive testing of polymers and composites. *NDT & E International* 98(1):130-133.
50. Smith RA (2009) Composite defects and their detection. *Materials Science and Engineering* 3(1): 103-143.
51. Solodov I (2014) Resonant acoustic nonlinearity of defects for highly-efficient nonlinear NDE *Journal of Nondestructive Evaluation* 33(2): 252-262.
52. Solodov I (2018) Nonlinear frequency shift and decay of local damage resonance: CAN Version. *Proceedings of Meetings on Acoustics* 34(1): 065001.
53. Solodov I and Busse G (2012) Multi-frequency defect selective imaging via nonlinear ultrasound. *Acoustical Imaging* 31(1): 385-398.
54. Solodov I, Rahammer M, Derusova D, et al. (2015) Highly-efficient and noncontact vibro-thermography via local defect resonance. *Quantitative InfraRed Thermography Journal* 12(1): 98-111.
55. Soutis C and Curtis PT (1996) Prediction of the post-impact compressive strength of CFRP laminated composites. *Composites Science and Technology* 56(6): 677-684.
56. Su Z, Wang X, Chen Z, et al. (2006) A built-in active sensor network for health monitoring of composite structures. *Smart Materials and Structures* 15(6): 1939-1949.
57. Su Z, Ye L and Lu Y (2006) Guided Lamb waves for identification of damage in composite structures: A review. *Journal of sound and vibration* 295(3-5): 753-780.
58. Tang HY, Winkelmann C, Lestari W, et al. (2011) Composite structural health monitoring through use of embedded PZT sensors. *Journal of Intelligent Material Systems and Structures* 22(8): 739-755.

59. Van Den Abeele KA, Carmeliet J, Ten Cate JA, et al. (2000) Nonlinear elastic wave spectroscopy (NEWS) techniques to discern material damage, Part II: Single-mode nonlinear resonance acoustic spectroscopy. *Journal of Research in Nondestructive Evaluation* 12(1): 31-42.
60. Van Den Abeele KA, Johnson PA and Sutin A (2000) Nonlinear elastic wave spectroscopy (NEWS) techniques to discern material damage, Part I: Nonlinear wave modulation spectroscopy (NWMS). *Journal of Research in Nondestructive Evaluation* 12(1): 17-30.
61. Vila M, Vander Meulen F, Dos Santos S, et al. (2004) Contact phase modulation method for acoustic nonlinear parameter measurement in solid. *Ultrasonics* 42(1-9): 1061-1065.
62. Wooh SC and Wei C (1999) A high-fidelity ultrasonic pulse-echo scheme for detecting delaminations in composite laminates. *Composites Part B: Engineering* 30(5): 433-444.
63. Wright P, Fu X, Sinclair I, et al. (2008) Ultra high resolution computed tomography of damage in notched carbon fiber-epoxy composites. *Journal of composite materials* 42(19): 1993-2002.
64. Yashiro S, Ogi K, Nakamura T, et al. (2013) Characterization of high-velocity impact damage in CFRP laminates: Part I–Experiment. *Composites Part A: Applied Science and Manufacturing* 48(1): 93-100.
65. Yoo S, Khatibi AA and Kandare E (2014) Durability of Embedded PZTs in Structural Health Monitoring Systems under Cyclic Loading. *Advanced Materials Research* 891(1): 1255-1260.
66. Zagrai A, Donskoy D, Chudnovsky A, et al. (2008) Micro-and macroscale damage detection using the nonlinear acoustic vibro-modulation technique. *Research in Nondestructive Evaluation* 19(2): 104-128.